Antiferromagnetic Spin Fluctuations and Structural Transition in Cluster Mott Insulator Candidate Nb_3Cl_8 Revealed by ^{93}Nb- and ^{35}Cl-NMR

Y. Z. Zhou[1,2], X. Han[1,2], J. Luo[1], D. T. Wu[3,4,1], A. F. Fang[5,6], B. Shen[3,4], B. J. Feng[1], Y. G. Shi[1*], J. Yang[1*], and R. Zhou[1*],

[1]*Institute of Physics, Chinese Academy of Sciences, and Beijing National Laboratory for Condensed Matter Physics, Beijing 100190, China*

[2]*School of Physical Sciences, University of Chinese Academy of Sciences, Beijing 100190, China*

[3]*Center for Neutron Science and Technology, Guangdong Provincial Key Laboratory of Magnetoelectric Physics and Devices, School of Physics, Sun Yat-Sen University, Guangzhou 510275, China*

[4]*State Key Laboratory of Optoelectronic Materials and Technologies, Sun Yat-Sen University, Guangzhou 510275, China*

[5]*School of Physics and Astronomy, Beijing Normal University, Beijing 100875, China*

[6]*Key Laboratory of Multiscale Spin Physics, Ministry of Education, Beijing Normal University, Beijing 100875, China*

(Received 30 December 2024; accepted manuscript online 7 February 2025)

Motivated by recent studies of the cluster Mott insulator candidate compound Nb_3Cl_8, this study performs ^{93}Nb and ^{35}Cl nuclear magnetic resonance (NMR) measurements to investigate the electron correlations. Below the structural transition temperature $T_s \sim 97$ K, all satellites of the ^{93}Nb NMR spectra split into three distinct peaks, which suggests symmetry lowering due to the structural transition and could be attributed to the change in the Nb-Nb bond-lengths of the Nb_3 clusters. The spin-lattice relaxation rate $1/T_1$ divided by the temperature T, $1/T_1T$, increases upon cooling to T_s for all Cl sites, whereas only the Knight shift K of Cl located at the center of the Nb_3 clusters exhibits a temperature dependence similar to that observed in magnetic susceptibility. These findings collectively demonstrate the existence of strong spin correlations between the Nb atoms in Nb_3Cl_8, which are closely associated with Mottness.

DOI: 10.1088/0256-307X/42/3/037303 CSTR: 32039.14.0256-307X.42.3.037303

In strongly correlated electron systems with half-filled bands, significant repulsive Coulomb interactions between electrons lead to Mott insulators.[1] Mott physics is a perennial hot topic in condensed matter physics because its appearance and related metal-insulator transitions are often intertwined with numerous exotic emergent phenomena, such as high-temperature (HT) superconductivity in doped cuprates[2] and quantum spin liquids (QSLs).[3] Cluster materials with partially filled bands have also been proposed as Mott insulators, where unpaired electrons are localized within clusters rather than only at the lattice sites.[4] For two-dimensional (2D) cluster Mott insulators with Kagome lattices, for example, $LiZn_2Mo_3O_8$ with Mo_3O_{13} cluster units, the spin states of the clusters are affected by electronic correlation and geometric frustration together.[5–8] Topological flat bands resulting from the Kagome lattices may further complicate this system.[9–11] The interplay between the spin, charge, and orbital degrees of freedom can lead to cluster Mottness evolving into more exotic states,[8] such as charge density waves (CDWs),[12,13] superconductivity,[14] and frustration-driven QSLs[15,16] in 1T-TaS_2.

Recently, there has been growing interest in the 2D van der Waals layered compound Nb_3Cl_8. The structure of Nb_3Cl_8 resembles that of Mo_3O_{13} cluster-based materials, featuring breathing Kagome lattices formed by the Nb_3Cl_{13} cluster units.[17] At a temperature of approximately $T_s \sim 97$ K, Nb_3Cl_8 undergoes a structural phase transition, and the magnetic susceptibility changes from para-magnetic to non-magnetic at low temperatures.[18] Previous nuclear magnetic resonance (NMR), X-ray diffraction (XRD), and terahertz spectroscopic studies reported that a structural transition occurred from the HT $P3\bar{m}1$ phase to the low-temperature (LT) $R3\bar{m}$ phase.[18–20] NMR measurements suggested charge disproportionation between adjacent layers, resulting in the disappearance of unpaired spins below T_s.[18] However, neutron and high-pressure XRD studies have suggested that the space group of the LT phase is monoclinic $C2/m$, accompanied by C_3 symmetry breaking within Nb_3 clusters.[21,22] Although the layer-stacking rearrangement is considered to be responsible for the phase transition, the nature of the structural transition in Nb_3Cl_8 remains controversial.

Most notably, each Nb_3 trimer in Nb_3Cl_8 shares an unpaired spin $S_{\text{eff}} = 1/2$, implying that the half-filled bands at E_F and Nb_3Cl_8 are potential cluster Mott insulators.[23] Electrical conductivity indicates that

*Corresponding author. Email: ygshi@iphy.ac.cn; yangjie@iphy.ac.cn; rzhou@iphy.ac.cn

© 2025 Chinese Physical Society and IOP Publishing Ltd. All rights, including for text and data mining, AI training, and similar technologies, are reserved.

Nb_3Cl_8 is an insulator.[24] DFT calculations suggested a half-filled flat band at the Fermi level (EF), whereas ARPES experiments revealed a large gap, indicating electron localization and an insulating ground state.[23] However, another ARPES study claimed a semiconducting ground state with a moderate ∼1.12 eV band gap because inversion symmetry breaking would open the gap in the Dirac cone.[25] Recent theories have suggested that the discrepancy between different studies can be attributed to band-selective normalization and that Nb_3Cl_8 is a cluster Mott insulator described by the single-band Hubbard model.[26,27] Although magnetic susceptibility exhibits a Curie-Weiss behavior at high temperatures, and a negative Weiss temperature indicates antiferromagnetic (AF) interactions between Nb_3 trimers,[18] microscopic investigations of spin correlations in Nb_3Cl_8 are still lacking. There is an ongoing debate regarding the ground state and electron correlations of Nb_3Cl_8. The clarification of this issue is of particular significance, given that numerous theoretical studies have predicted novel properties such as possible QSLs,[16,26,28] monolayer ferromagnetism,[29] topological insulation,[30] unconventional superconductivity through doping of the Mott state,[31] and even potential novel properties in heterostructures.[32,33]

In this study, both ^{93}Nb- and ^{35}Cl-NMR measurements are conducted to investigate the electron correlations and local structures in Nb_3Cl_8. In the LT phase below T_s, the satellite lines of ^{93}Nb-NMR spectra split into three lines with nearly identical spectral weights, indicating that there exist three inequivalent Nb sites and the bond-lengths of the Nb_3 clusters change owing to structural transition. In the HT phase, the spin-lattice relaxation rate $1/T_1$ divided by the temperature T, $1/T_1T$, shows a monotonic increase for all the Cl sites as the temperature decreases towards T_s. However, only the Knight shift of Cl located at the center of the Nb_3 cluster displays a temperature dependence similar to that observed in the magnetic susceptibility, implying that the Nb_3 trimer shares an unpaired spin $S_{\text{eff}} = 1/2$. These results provide microscopic evidence for AF spin fluctuations at high temperatures in Nb_3Cl_8 and suggest the existence of Mott physics. Furthermore, the findings of this study highlight how geometric frustration influences electronic correlations through its unique cluster Kagome structure and offer new insights into its phase transition and ground state.

The Nb_3Cl_8 single crystals used in this study were synthesized using the $PbCl_2$ flux method.[18] The typical dimensions of a single crystal were $2\times2\times0.1$ mm. The ^{93}Nb- and ^{35}Cl-NMR spectra were obtained through fast Fourier transform (FFT) summation. The spin echo was observed using a $\pi/2$-τ-π pulse sequence on a phase-coherent spectrometer. A $\pi/2 = 5\,\mu$s pulse was employed with pulse intervals $\tau = 150\,\mu$s for ^{35}Cl and 75 μs for ^{93}Nb nuclei. The spin-lattice relaxation time (T_1) was determined using the saturation-recovery method.

Figure 1(a) shows the ^{93}Nb NMR spectrum at 78 K under a fixed magnetic field $B_0 = 4$ T along the c-axis. For the nucleus with the nuclear quadrupole moment Q, the total Hamiltonian under the field can be written as

$$\begin{aligned}\mathcal{H} &= \mathcal{H}_0 + \mathcal{H}_{\text{Q}} \\ &= \gamma\hbar \boldsymbol{I}\cdot\boldsymbol{B}_0(1+K) + \frac{e^2qQ}{4I(I+1)} \\ &\quad\cdot\left[(3I_z^2 - I^2) + \frac{1}{2}\eta(I_+^2 + I_-^2)\right], \end{aligned} \tag{1}$$

where K is the Knight shift, $^{93}\gamma = 10.405$ MHz/T is the nuclear gyromagnetic ratio, eq is the electric field gradient (EFG) along the principal axis, and $\eta = \left|\frac{V_{xx}-V_{yy}}{V_{xx}+V_{yy}}\right|$ is the EFG asymmetry parameter. As ^{93}Nb nucleus had a spin $I = 9/2$, the NMR spectrum was expected to exhibit nine resonance peaks: one central peak and eight first-order satellites. In the HT phase above T_s, ^{93}Nb had only one crystallographic site, as shown in Fig. 1(b). However, at $T = 78$ K, which is below T_s, all the satellite peaks split into three peaks, except for the central line. Figure 1(c) presents an enlarged view of the lowest frequency satellite peak. The area ratio of the three peaks was approximately 1:1:1, indicating the presence of three distinct Nb sites in the LT phase. Table 1 shows the obtained nuclear quadrupole resonance (NQR) frequency ν_Q, K, η and the relative abundance ratio (AO) for the three ^{93}Nb sites in the ^{93}Nb NMR spectrum. It should be noted that in previous NMR measurements, only two sets of split peaks with an area ratio close to 1:1 were observed, which were interpreted as two alternating nonmagnetic layers of Nb_3 clusters owing to charge disproportionation.[18] In this study, a much smaller single-crystal sample was employed and a magnetic field strength of only 4 T was applied, resulting in narrower NMR lines. Considering that the two higher frequency peaks were closely spaced, as shown in Fig. 1(c), they were difficult to resolve using larger samples at higher fields.

The presence of three distinct Nb positions in the LT phase is discussed in this section. A possible explanation is that the Nb_3 cluster maintained the same equilateral triangular structure as that in the HT phase; however, the Nb–Nb bond lengths varied along the c-direction, as shown in Fig. 2(a). Alternatively, it is plausible that the Nb_3 clusters deviated from the equilateral triangle, resulting in three inequivalent Nb sites, as shown in Fig. 2(b). Neutron scattering and XRD studies suggested a monoclinic $C2/m$ space group for the LT phase and an isosceles triangular structure for the Nb_3 cluster.[21] Such a Nb_3 cluster configuration would result in only two different Nb sites with an atomic ratio of 1:2. Therefore, another possibility is that the Nb_3 clusters formed an isosceles triangular structure along the c-axis, but with different top angles ϕ for adjacent layers, as shown in Fig. 2(c). Further high-resolution XRD studies are required to fully determine the LT structure of Nb_3Cl_8. In addition, the central lines of the three Nb sites coincided, as shown in Fig. 1(a), indicating they had identical Knight shifts. This is consistent with the fact that the magnetic susceptibility of the LT phase was nearly zero, which caused no spin shift at any Nb site. The results of this study reveal the appearance of inequivalent Nb_3 clusters in the LT phase, which disrupted shared unpaired spins within overlapping molecular orbitals and consequently led to non-magnetic behavior.

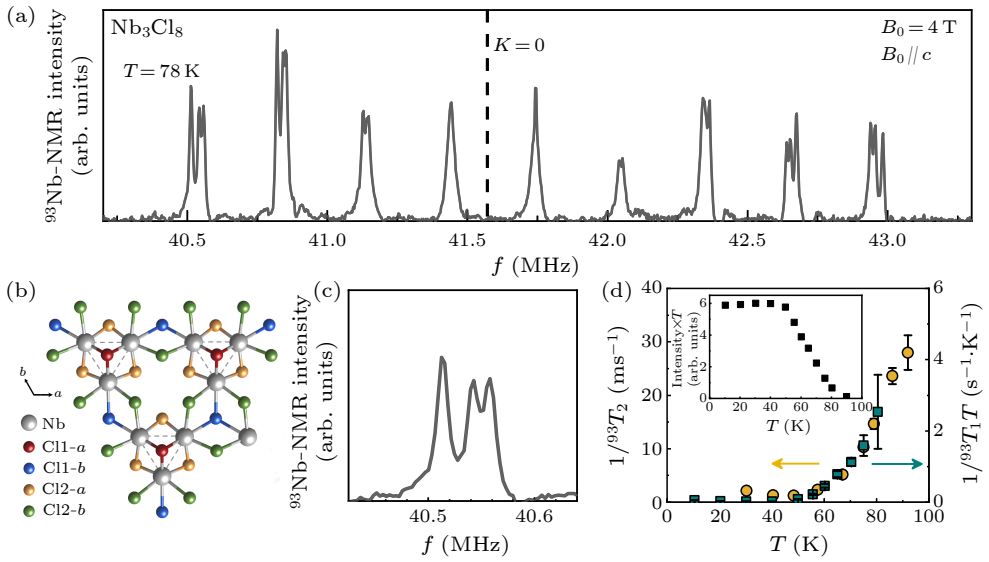

Fig. 1. (a) ^{93}Nb NMR spectrum at 78 K with the applied magnetic field $B_0 = 4$ T. The dashed line shows the Knight shift $K = 0$. (b) Kagome lattice structure of monolayer Nb_3Cl_8. (c) Enlarged view of the lowest frequency satellite peak of the ^{93}Nb NMR spectrum. (d) Temperature variation of the $1/T_1T$ (square), $1/T_2$ (circle), and spectrum weight (inset) of ^{93}Nb.

Table 1. NMR parameters for the ^{93}Nb spectrum at 78 K.

Site	ν_Q	K(%)	η	AO
Nb1	0.617	0.44	0.019	∼1/3
Nb2-1	0.603	0.44	0.027	∼1/3
Nb2-2	0.596	0.44	0.027	∼1/3

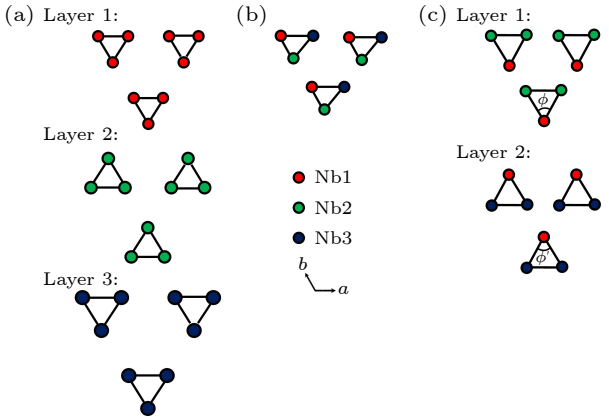

Fig. 2. Possible Nb_3 trimer structures within adjacent layers in the LT phase. (a) The Nb_3 trimers remained equilateral triangles, but had different Nb–Nb bond lengths for adjacent layers, resulting in a 3c periodicity along c-axis. Notably, this configuration did not break rotational symmetry. (b) Distinct Nb–Nb bond lengths for the Nb_3 trimer within one layer. (c) The Nb_3 trimer had an isosceles triangle configuration in each layer but with different top angles ϕ for adjacent layers, leading to a 2c period along c-axis. It is noted that both (b) and (c) resulted in rotational symmetry breaking. For all cases, three different Nb sites were observed in the NMR spectra.

With increasing temperature, the ^{93}Nb NMR signal intensity decreased significantly, owing to a sharp increase in the spin–spin relaxation rate $1/T_2$ and $1/T_1T$ near the structural phase transition, as shown in Fig. 1(d). These observations strongly suggest a rapid enhancement of spin fluctuations near T_s with increasing temperature. As $^{93}T_2$ was significantly shorter than the dead time of the spectrometer (∼5 μs), the ^{93}Nb-NMR signal was completely wiped out above T_s. Therefore, to gain insights into the electron correlations in the HT phase, ^{35}Cl-NMR measurements were performed. All Cl sites were far from the Nb atoms; thus, the hyperfine coupling between ^{35}Cl nuclei and Nb electron spins was significantly weaker, which resulted in a significantly longer spin–spin relaxation time for ^{35}Cl NMR signals and ensured their persistence in the HT phase.

Figure 3 shows the ^{35}Cl NMR spectra at different temperatures under an applied magnetic field $B_0 = 16$ T along the c-axis. In Nb_3Cl_8, there were two different Cl crystallographic sites, Cl1 was at the center of the Nb-triangle

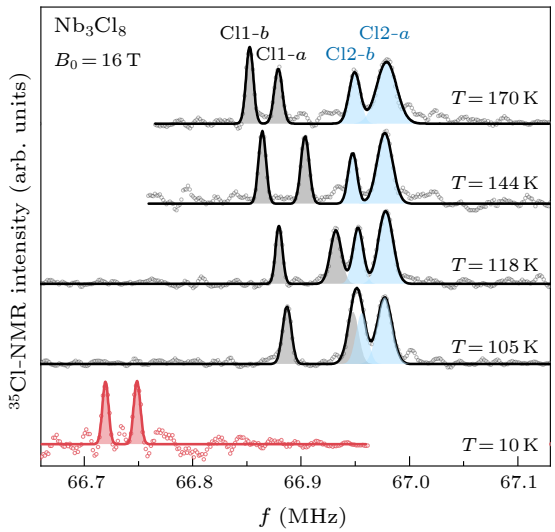

Fig. 3. Temperature dependence of the ^{35}Cl-NMR spectra under an applied magnetic field $B_0 = 16$ T for Nb_3Cl_8 along the c-axis. The solid curves and shaded regions are the fittings for different Cl sites by the Gaussian function.

and Cl2 was beside the Nb-triangle, as shown in Fig. 1(b). As a result of the different Nb–Nb bond lengths within the layer, both the Cl1 and Cl2 sites were further divided into two types: Cl1-a and Cl2-a near the shorter Nb-Nb bond-length and Cl1-b and Cl2-b near the longer Nb-Nb bond-length. For a ^{35}Cl nucleus with a spin of $I = 3/2$, each Cl site should exhibit three transition lines in the NMR spectrum; thus, the spectrum should have 12 lines overall. However, because of the limitations imposed by the single-crystal size, no satellite peaks were observed; instead, only four central lines were visible above T_s. The following section discusses the identification of the ^{35}Cl sites in the NMR spectra. The magnetic-field dependence of the ^{35}Cl-NMR spectra was measured and the EFG asymmetry parameter η was obtained for each Cl peak. The two lower-frequency peaks exhibited a near-zero asymmetry parameter η, whereas the two higher frequency peaks displayed finite η values (further details and additional results can be found in the Supplementary Material[34]). As Cl1-a and Cl1-b were located in a symmetric EFG environment, the η for the Cl1-a and Cl1-b sites should be zero.

Therefore, we assigned the two lower frequency peaks as corresponding to Cl1 sites, while the two higher frequency peaks to Cl2 sites. The Cl-a and Cl-b were further distinguished by comparing their hyperfine coupling constants, as described below. Upon decreasing the temperature below T_s, an abrupt change in the NMR spectra was observed, indicating a first-order structural transition. Only two peaks, corresponding to the Cl1-a and Cl1-b sites, were observed at 10 K. A possible reason for this change in the spectra is that the Cl2 sites had a longer T_1, resulting in an undetectable NMR signal for Cl2.

The Knight shift K was defined as $K = (f - f_{2nd} - \gamma B_0)/\gamma B_0$, where f is the observed resonance frequency, $\gamma = 4.17169$ MHz/T is the gyromagnetic ratio of ^{35}Cl, and f_{2nd} is the second-order quadrupole shift (more details can be found in the Supplementary Material[34]). Figure 4(a) shows the temperature dependence of K for all Cl sites. The most striking feature is that K values for Cl1 and Cl2 exhibited completely different variations. For the Cl1-a and Cl1-b sites, K exhibited Curie-Weiss behavior, which is consistent with the temperature variation of magnetic susceptibility χ.[18] Here, K is expressed as $K = K_{spin} + K_{orb}$, where $K_{spin} = A_{spin}\chi_{spin}$ is proportional to the static spin susceptibility χ_{spin} by the hyperfine coupling constant A_{spin}, while K_{orb} is the contribution from orbital (Van Vleck) susceptibility and is typically temperature independent. Plotting K as a function of χ showed that they had a linear relationship above T_s,[34] indicating the intrinsic Curie-Weiss behavior of χ_{spin}. The A_{spin} values for Cl1-a and Cl1-b were different, allowing discrimination between the two Cl sites. As Cl1 was located at the center of the Nb_3 triangle, the findings of this study provide clear microscopic evidence of the presence of unpaired spins in the molecular orbitals of each Nb_3 trimer. By fitting K with the Curie-Weiss function, as shown in Fig. 4(a), the Weiss temperature $\theta = -20 \pm 10$ K was obtained. The negative value of θ suggests AF interactions between Nb_3 trimers. For the Cl2-a and Cl2-b sites, K was nearly temperature-independent. This may be because the hyperfine coupling constant was almost zero for the Cl2 sites.[34]

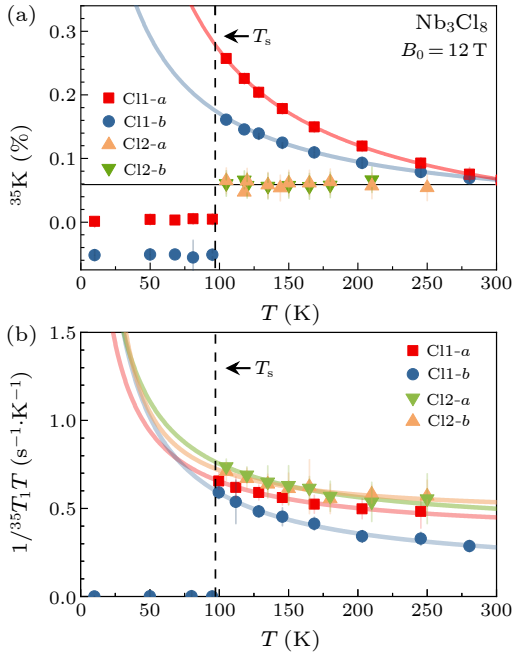

Fig. 4. Temperature dependence of K(a) and $1/T_1T$(b) for different ^{35}Cl sites. The dashed line indicates the structural phase transition temperature T_s. The solid lines are Curie-Weiss fits.

Finally, this section discusses the spin correlations based on the temperature dependence of $1/T_1T$ as shown in Fig. 4(b). For all Cl sites, $1/T_1T$ increased with decreasing temperature until it reached T_s, followed by a sudden transition to an extremely low value below T_s. Notably, this value was approximately 430 times smaller than that observed for ^{93}Nb site [Fig. 1(d)]. Consequently, the ^{93}Nb-NMR signal in the HT phase was wiped out because of the pronounced fluctuations of the Nb 4d electron spins. These findings strongly support the presence of spin fluctuations in the HT phase and provide compelling evidence that Nb_3Cl_8 is a cluster Mott insulator. In general, $1/T_1T$ is proportional to the imaginary part of the dynamic susceptibility perpendicular to the applied field ($\chi''_\perp(q,\omega)$), and can be written as

$$\frac{1}{T_1T} \propto \sum_q |A(\boldsymbol{q})|^2 \frac{\chi''_\perp(\boldsymbol{q},\omega)}{\omega}, \tag{2}$$

where $A(\boldsymbol{q})$ denotes the wave vector $\boldsymbol{q}$ dependent hyperfine coupling constant and ω is the NMR frequency. K probes the static magnetic susceptibility at $\boldsymbol{q} = 0$, whereas $1/T_1$ is sensitive to spin fluctuations at $\boldsymbol{q} \neq 0$. There was a peak around the finite wave vector (due to AF spin fluctuations). Therefore, $A(\boldsymbol{q})$ in $1/T_1T$ was significant for all Cl sites, although A was nearly zero for the Cl2 sites in the Knight shift, as observed for $YBa_2Cu_3O_{6.63}$.[35] To gain insight into spin fluctuations, $1/T_1T$ can be written as $1/T_1T = (1/T_1T)_0 + (1/T_1T)_{AF}$. The first term $(1/T_1T)_0$ represents the contribution from the non-correlated electrons and is related to the density of states at the EF. The second term $(1/T_1T)_{AF}$ represents the contribution of AF

spin fluctuations. In the case of 2D AF spin fluctuations, $(1/T_1T)_{\rm AF}$ follows the Curie-Weiss T dependence[36]

$$(1/T_1T)_{\rm AF} \propto \frac{C}{T+\theta}. \quad (3)$$

As shown in Fig. 4(b), the experimental data are well-fitted by Eq. (3). The obtained $\theta \sim -30 \pm 20$ K suggests that the AF spin fluctuations would be persistently enhanced if the structural transition does not occur at $T_{\rm s} \sim 97$ K. The $1/T_1T$ results also imply that the structural transition was not triggered by the AF spin correlations. However, no magnetic transition signature was observed in the powder sample, in which the structural transition was suppressed.[18] Therefore, the results of this study indicate that powdered Nb_3Cl_8 could be a QSL candidate owing to its strong electron spin correlations and Kagome structure. Further investigations are required to fully elucidate the ground state properties of powdered Nb_3Cl_8.

In conclusion, this study investigated the electron correlations and local structures in Nb_3Cl_8 using ^{93}Nb- and ^{35}Cl-NMR measurements. In the LT phase, the satellite lines of the ^{93}Nb-NMR spectra exhibited three lines with nearly identical spectral weights, indicating the presence of three distinct Nb sites. The findings of this study suggest that the bond-length variations result in the inequivalence among Nb_3 clusters. In the HT phase, $1/T_1T$ exhibited a Curie-Weiss temperature dependence for all Cl sites as the temperature decreased towards $T_{\rm s}$. The Knight shift of Cl located at the center of the Nb_3 cluster also showed a similar temperature dependence as that observed in the magnetic susceptibility, implying an unpaired spin shared by the Nb_3 trimer. Thus, the results of this study indicate that AF spin fluctuations developed at high temperatures in Nb_3Cl_8. It is anticipated that this study will inspire further experimental measurements of Nb_3Cl_8 to identify novel phenomena and the related Mott physics.

Acknowledgements. This study was supported by the National Key Research and Development Projects of China (Grant Nos. 2022YFA1403402, 2023YFA1406103, 2024YFA1409200, 2024YFA1611302, and 2023YFF0718400), the National Natural Science Foundation of China (Grant Nos. 12374142, 12304170, W2411004, and 12374197), the Beijing Natural Science Foundation (Grant No. JQ23001), the Beijing National Laboratory for Condensed Matter Physics (Grant No. 2024BNLCMPKF005), and the Guangdong Basic and Applied Basic Research Foundation (Grant No. 2023B151520013). This study was supported by the Synergetic Extreme Condition User Facility (SECUF, https://cstr.cn/31123.02.SECUF).

References

[1] Mott N F 1968 *Rev. Mod. Phys.* **40** 677
[2] Lee P A, Nagaosa N, and Wen X G 2006 *Rev. Mod. Phys.* **78** 17
[3] Pustogow A, Bories M, Löhle A, Rösslhuber R, Zhukova E, Gorshunov B, Tomić S, Schlueter J A, Hübner R, Hiramatsu T, Yoshida Y, Saito G, Kato R, Lee T, Dobrosavljević V, Fratini S, and Dressel M 2018 *Nature Mater.* **17** 773
[4] Chen G and Lee P A 2018 *Phys. Rev. B* **97** 035124
[5] Gall P, Al Rahal Al Orabi R, Guizouarn T, and Gougeon P 2013 *J. Solid State Chem.* **208** 99
[6] Torardi C C and McCarley R E 1985 *Inorg. Chem.* **24** 476
[7] Mourigal M, Fuhrman W T, Sheckelton J P, Wartelle A, Rodriguez-Rivera J A, Abernathy D L, Mc-Queen T M, and Broholm C L 2014 *Phys. Rev. Lett.* **112** 027202
[8] Sheckelton J P, Neilson J R, Soltan D G, and McQueen T M 2012 *Nat. Mater.* **11** 493
[9] Liu H, Meng S, and Liu F 2021 *Phys. Rev. Mater.* **5** 084203
[10] Regnault N, Xu Y, Li M R, Ma D S, Jovanovic M, Yazdani A, Parkin S S P, Felser C, Schoop L M, Ong N P, Cava R J, Elcoro L, Song Z D, and Bernevig B A 2022 *Nature* **603** 824
[11] Yin I X, Lian B, and Hasan M Z 2022 *Nature* **612** 647
[12] Sipos B, Kusmartseva A F, Akrap A, Berger H, Forro L, and Tutis E 2008 *Nat. Mater.* **7** 960
[13] Thomson R E, Burk B, Zettl A, and Clarke J 1994 *Phys. Rev. B* **49** 16899
[14] Li L J, Lu W J, Liu Y, Qu Z, Ling L S, and Sun Y P 2013 *Physica C* **492** 64
[15] Law K T, and Lee P A 2017 *Proc. Natl. Acad. Sci.* **114** 6996
[16] Balents L 2010 *Nature* **464** 199
[17] Magonov S N, Zoennchen P, Rotter H, Cantow H J, Thiele G, Ren J, and Whangbo M H 1993 *J. Am. Chem. Soc.* **115** 2495
[18] Haraguchi Y, Michioka C, Ishikawa M, Nakano Y, Yamochi H, Ueda H, and Yoshimura K 2017 *Inorg. Chem.* **56** 3483
[19] Pasco C M, El Baggari I, Bianco E, Kourkoutis L F, and McQueen T M 2019 *ACS Nano* **13** 9457
[20] Kim J, Lee Y, Choi Y W, Jung T S, Son S, Kim J, Choi H J, Park J G, and Kim J H 2023 *ACS Omega* **8** 14190
[21] Sheckelton J P, Plumb K W, Trump B A, Broholm C L, and McQueen T M 2017 *Inorg. Chem. Front.* **4** 481
[22] Jiang Z, Jiang D, Wang Y, Li C, Liu K, Wen T, Liu F, Zhou Z, and Wang Y 2022 *Sci. China Phys. Mech. Astron.* **65** 278211
[23] Gao S, Zhang S, Wang C, Tao W, Liu J, Wang T, Yuan S, Qu G, Pan M, Peng S, Hu Y, Li H, Huang Y, Zhou H, Meng S, Yang L, Wang Z, Yao Y, Chen Z, Shi M, Ding H, Jiang K, Li Y, Shi Y G, Weng H M, and Qian T 2023 *Phys. Rev. X* **13** 041049
[24] Yoon J, Lesne E, Sklarek K, Sheckelton J, Pasco C, Parkin S S P, McQueen T M, and Ali M N 2020 *J. Phys.: Condens. Matter* **32** 304004
[25] Sun Z, Zhou H, Wang C, Kumar S, Geng D, Yue S, Han X, Haraguchi Y, Shimada K, Cheng P, Chen L, Shi Y, Wu K, Meng S, and Feng B 2022 *Nano Lett.* **22** 4596
[26] Hu J Y, Zhang X F, Hu C, Sun J, Wang X Q, Lin H Q, and Li G 2023 *Commun. Phys.* **6** 172
[27] Grytsiuk S, Katsnelson M I, van Loon E G C P, and Rösner M 2024 *npj Quantum Materials* **9** 8
[28] Kasahara Y, Ohnishi T, Mizukami Y, Tanaka O, Ma S, Sugii K, Kurita N, Tanaka H, Nasu J, Motome Y, Shibauchi T, and Matsuda Y 2018 *Nature* **559** 227
[29] Jiang J, Liang Q, Meng R, Yang Q, Tan C, Sun X, and Chen X 2017 *Nanoscale* **9** 2992
[30] Bradlyn B, Elcoro L, Cano J, Vergniory M G, Wang Z, Felser C, Aroyo M I, and Andrei Bernevig B 2017 *Nature* **547** 298
[31] Zhang Y, Gu Y, Weng H, Jiang K, and Hu J 2023 *Phys. Rev. B* **107** 035126
[32] Wu H, Wang Y, Xu Y, Sivakumar P K, Pasco C, Filippozzi U, Parkin S S P, Zeng Y J, McQueen T, and Ali M N 2022 *Nature* **604** 653
[33] Ando F, Miyasaka Y, Li T, Ishizuka J, Arakawa T, Shiota Y, Moriyama T, Yanase Y, and Ono T 2020 *Nature* **584** 373
[34] See Supplemental Materials for details.
[35] Takigawa M, Reyes A P, Hammel P C, Thompson J D, Heffner R H, Fisk Z, and Ott K C 1991 *Phys. Rev. B* **43** 247
[36] Moriya T 1985 *Spin Fluctuations in Itinerant Electron Magnetism* (Springer-Verlag)